C_1-symmetric [Ir(C^N^1)(C^N^2)(N^O)]-*tris*-heteroleptic Ir(III)-complexes with horizontal orientation for efficient near-infrared (NIR) polymer light-emitting diodes (PLEDs)

Wentao Li,‡[a] Tiezheng Miao,‡[a] Baowen Wang,[a] Jiaxiang Liu,[a] Xingqiang Lü,[a,*] Guorui Fu,[a,c*] Weixu Feng[b,*] and Wai-Yeung Wong[c,*]

Using conventionally *fac*-[Ir(C^N)$_3$]-homoleptic or [Ir(C^N)$_2$(L^X)]-*bis*-heteroleptic iridium(III)-complexes with NIR-phosphorescence (NIR = near infrared) as dopants, the realization of their reliable NIR-OLEDs/PLEDs (organic/polymer light-emitting diodes) with high-performance remains a real challenge. In this study, taking the **Hqibt** (1-(benzo[*b*]-thiophen-2-yl)-isoquinoline) as the HC^N^1 ligand, **Hppy** (phenyl-4-yl)pyridine) as the HC^N^2 ligand and the **Br-Hpic** (5-Br-picolinic acid) or **Hpic** (picolinic acid) as the N^O-ancillary, two novel C_1-symmetric [Ir(C^N^1)(C^N^2)(N^O)]-*tris*-heteroleptic iridium(III)-complexes [Ir(iqbt)(ppy)(pic)] (**1**) and [Ir(iqbt)(ppy)(Br-pic)] (**2**) are molecularly designed, respectively, where the large TDM (transition dipole moment) and the strengthened ^{3}MLCT (metal-to-ligand charge transfer) effect are founded to afford their good NIR-phosphorescent efficiency ((Φ_{PL} = 0.27 for **1** (λ_{em} = 698 nm); 0.21 for **2** (λ_{em} = 696 nm)). Moreover, in their doped EMLs (emitting layers), the preferentially horizontal orientation of the TDMs is motivated, from which, their **NIR-PLEDs-1-2** exhibit the attractively high efficiency (η_{EQE}^{max} = 3.1-4.7%; λ_{em} = 698 nm) apart from the almost negligible (< 5%) efficiency roll-off. This finding engenders C_1-symmetric [Ir(C^N^1)(C^N^2)(N^O)]-*tris*-heteroleptic Ir(III)-complexes a promising opportunity to low-cost, large-area and scalable NIR-PLEDs.

1. Introduction

Contributed from the strong spin-orbit coupling (SOC)[1] of Ir(III) nucleus, neutral cyclometalated Ir(III)-complexes endow desirably chemical inertness and almost 100% internal quantum efficiency (η_{int}). Moreover, associated with the ^{3}LC/^{3}MLCT-admixed (LC = ligand-centered, MLCT = metal-to-ligand charge transfer) transitions, their lowest triplet excited-state (^{1}T) level is smoothly modulated by the ligands' engineering,[2] enabling the realization of high-efficiency organic/polymer light-emitting diodes (OLEDs/PLEDs)[3] with the phosphorescent wavelengths across the whole visible regime. However, in sharp contrast to high external quantum efficiency (η_{EQE}) of ~20% for blue-OLEDs[4] or ~30% for green[5]/red ones,[6] the development of Ir(III)-complex-based efficient NIR-OLEDs/PLEDs (NIR = near-infrared, λ_{em} > 690 nm) is still an unaddressed issue,[7] despite their emerging importance in night-vision[8] and information security[9] devices, telecommunication[10] or bio-analysis.[11] According to the theoretically fundamental equation[12] of η_{EQE},

$$\eta_{EQE} = \eta_{PL} \times \eta_{exciton} \times \eta_{eh} \times \eta_{out} \quad (1)$$

η_{PL} is the emitter's radiative quantum yield, $\eta_{exciton}$ is the radiative exciton ratio, η_{eh} is the carriers-recombination efficiency and η_{out} is the light out-coupling efficiency. For Ir(III)-complex-based NIR-emitters capable of both singlet and triplet excitions' harvesting with $\eta_{exciton}$ of 100%, it remains a great challenge to enhance their inherent η_{PL} in the limit of the so-called "energy-gap law".[13] Moreover, even with η_{eh} of 100% from specific state-of-the-art NIR-OLED/PLED structure that shows a perfect carriers' balance, its η_{EQE} is further constrained by the theoretical prediction of η_{out} ~20%, due to the absence of any extra light out-coupling technique,[14] giving rise to another parallel challenge.

Forward to the light out-coupling apart from micro-lens arrays,[15] gratings[16] or other physical methods,[17] an alternative approach[18] to increasing the η_{out} is through the preference of molecular orientation of one specific emitter in the EML (emitting layer). Since the first observation of oriented phosphorescent species by M. Flämmich et al[19] in 2011, *fac*-[Ir(C^N)$_3$]-homoleptic[20] and [Ir(C^N)$_2$(L^X)]-*bis*-heteroleptic[21] Ir(III)-complexes were developed to boost the desirable η_{out} with a preferential alignment of their transition dipole moment (TDM). As an empirical rule, Ir(C^N)$_2$(L^X)]-*bis*-heteroleptic Ir(III)-complexes[21] with C_1- or C_2-axis induced by the L^X-symmetry or not, are demonstrated to offer relatively higher η_{out} values than those of their *fac*-[Ir(C^N)$_3$]-homoleptic C_3-analogues,[20] probably because the average TDM vectors of lower-symmetric Ir(III)-complexes in the corresponding EMLs are disproportionately horizontal in relative to the substrate. Unfortunately, this proof-of-concept strategy in population with visible-lights,[19-22] is not yet available for Ir(III)-complex-based NIR-emitting counterparts, where undoubtedly, besides the inherent factor of high η_{PL} in the NIR-emissive gamut, effective carriers' trapping/recombination and substantial light extraction should also be considered to develop their efficient NIR-OLEDs/PLEDs.

[a]*School of Chemical Engineering, Northwest University, Xi'an 710069, Shaanxi, China. E-mail: lvxq@nwu.edu.cn*
[b]*School of Chemistry and Chemical Engineering, Northwestern Polytechnical University, Xi'an 710029, Shaanxi, China. E-mail: fwxdk@nwpu.edu.cn*
[c]*Department of Applied Biology and Chemical Technology, The Hong Kong Polytechnic University, Hung Hom, Hong Kong, China. E-mail: guorui.fu@polyu.edu.hk; wai-yeung.wong@polyu.edu.hk*
†Electronic Supplementary Information (ESI) available: [Starting materials and characterization; NMR, UV, PL]. See DOI: 10.1039/x0xx00000x
‡These authors contributed equally and should be considered *co*-first authors.

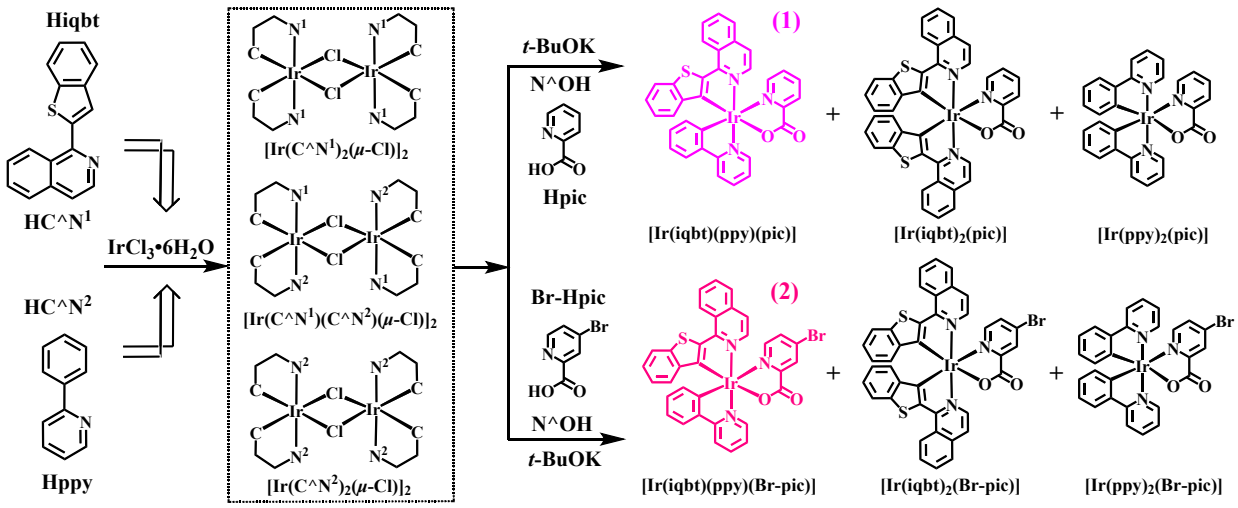

Scheme 1 Synthetic scheme of the *in situ* formed μ-chloro-bridged dimer intermediates and their corresponding [Ir(C^N)$_2$(N^O)]-*bis*-heteroleptic by-products and [Ir(C^N^1)(C^N^2)(N^O)]-*tris*-heteroleptic Ir(III)-complexes **1**-**2**

As a matter of fact, accompanying with conventional *fac*-[Ir(C^N)$_3$]-homoleptic[23] or [Ir(C^N)$_2$(L^X)]-heteroleptic[24] Ir(III)-complexes used for reliable vacuum-deposited or solution-processed NIR-OLEDs/PLEDs, C_1-symmetric *tris*-heteroleptic Ir(III)-complexes composed of an Ir(III) ion and three different ligands are rarely carried forward to the NIR-emitting system,[25] despite the cognitions of their appreciable vivid-visible-devices' (λ_{em} = 465-600 nm) performance on [Ir(C^N^1)(C^N^2)(O^O)]-,[26] [Ir(C^N)(N^N^1)(N^N^2)]-,[27] [Ir(C^N^1)(C^N^2)(C^N^3)]-[28] or [Ir(C^N)(C^C)(O^O)]-[29] neutral system. Herein, two novel [Ir(C^N^1)(C^N^2)(N^O)]-*tris*-heteroleptic Ir(III)-complexes (**Scheme 1**) with the C_1-symmetry are molecularly designed to fill in that blank. On one hand, Ruled by the so-called "energy-gap law",[13] the rate of non-radiative decay (k_{nr}) has an inverse dependence on the ^{1}T level. The radiative rate constant (k_r) is exponentially relative to the ^{1}T-transitted energy and concurrently proportional to the square of TDM ($k_r \in$ TDM^2) according to the electronic transition theory.[30] Therefore, if large TDMs can generate from the C_1-symmetric [Ir(C^N^1)(C^N^2)(N^O)]-*tris*-heteroleptic Ir(III)-complexes with desirable NIR-emissions, the TDM-induced fast radiative transition could challenge their inherent low η_{PL}. On the other hand, the TDM may also have some correlation[22] with the molecular orientation of their-doping EMLs, from which, effective NIR-light out-coupling should be motivated for their resultant NIR-OLEDs/PLEDs.

2. Experimental section

Synthesis of the μ-chloro-bridged dimer intermediates including [Ir(iqbt)(ppy)(μ-Cl)]$_2$

To a stirred solution of the equimolar amount of the C^N^1 ligand **Hiqbt** (288 mg, 1.10 mmol) and **Hppy** (170 mg, 1.10 mmol) in 2-ethoxyethanol/H_2O (30 mL; 3:1 (v/v)), $IrCl_3 \cdot 3H_2O$ (353 mg, 1.00 mmol) was added, the resultant mixture was heated to 110 °C and continuously stirred under a N_2 atmosphere for 24 h. After cooling to room temperature, the saturated brine (50 mL) was added, and the dark-brown suspension was filtered. Further washing with D. I. water, diethyl ether and hexane, and drying at 45 °C under vacuum to constant weight, the *in situ* formed μ-chloro-bridged dimer intermediates containing **[Ir(iqbt)(ppy)(μ-Cl)]$_2$** as brown solid products were collected and directly used in the following. Yield: 514 mg (80%).

Synthesis and isolation of the [Ir(iqbt)(ppy)(pic)] (1)

To a solution of the *in situ* formed μ-chloro-bridged dimer intermediates (257 mg, 0.2 mmol) in anhydrous CH_2Cl_2 (30 mL), *t*-BuOK (3.0 equiv.) and **Hpic** (3.0 equiv.) were added, and the reaction mixture was continuously stirred at room temperature under a N_2 atmosphere for 24 h. After drying under vacuum, the residue was further purified by flash column chromatography on SiO_2 gel with a mixed solvent (CH_2Cl_2/MeOH (v/v = 50:1)), to give the desirable product and the by-products, respectively.

For the first eluted **[Ir(iqbt)$_2$(pic)]** (red polycrystalline solid; R_f = 0.56): Yield: 62 mg (28%). Calcd for $C_{40}H_{24}IrN_3O_2S_2$: C, 57.54; H, 2.90; N, 5.03%. Found: C, 57.59; H, 2.87; N, 4.93%. ^{1}H NMR (400 MHz, $CDCl_3$): δ (ppm) 9.09 (d, 1H, -Py), 9.02 (d, 1H, -Py), 8.73 (d, 1H, -Py), 8.26 (d, 1H, -Py), 7.92 (d, 1H, -Py), 7.77 (m, 9H, -Ph), 7.38 (d, 1H, -Ph), 7.30 (m, 2H, -Py), 7.17 (m, 2H, -Ph), 7.06 (t, 1H, -Py), 6.79 (t, 1H, -Ph), 6.63 (t, 1H, -Ph), 6.49 (t, 1H, -Ph), 6.08 (d, 1H, -Ph). ESI-MS (in CH_2Cl_2): *m/z*: 835.09 (100%; [M-H]$^+$). This characterization result was identical to those in the literature.[31]

For the second eluted **[Ir(iqbt)(ppy)(pic)]** (**1**; reddish orange polycrystalline solid; R_f = 0.44): Yield: 35 mg (25%). Calcd for $C_{34}H_{22}IrN_3O_2S$: C, 56.03; H, 3.04; N, 5.77%. Found: C, 56.13; H, 3.12; N, 5.65%. FT-IR (KBr cm^{-1}): 3408 (w), 3053 (w), 2918 (w), 2849 (w), 1637 (m), 1597 (m), 1577 (m), 1560 (w), 1544 (w), 1502 (w), 1479 (w), 1438 (m), 1417 (s), 1340 (m), 1309 (w), 1286 (w), 1234 (w), 1163 (w), 1128 (w), 1089 (w), 1066 (m), 1049 (w), 1024 (w), 970 (w), 920 (w), 850 (w), 842 (w), 804 (w), 761 (vs), 729 (s), 694 (m), 686 (s), 663 (w), 629 (w), 565 (w), 542 (w), 501 (w), 472 (w), 428 (m). ^{1}H NMR (400 MH$_Z$, $CDCl_3$): δ (ppm) 9.05 (d, 1H, -Py), 8.96 (d, 1H, -Py), 8.34 (d, 1H, -Py for pic), 7.95 (d, 1H, -Py), 7.82 (q, 2H, -Py), 7.78 (t, 2H, -Py), 7.72 (m, 2H, -Ph), 7.66 (q, 2H, -Ph), 7.39 (t, 1H, -Ph), 7.25 (d, 1H, -Ph), 7.21 (t, 1H, -Ph), 7.14 (t, 1H, -Ph), 7.11 (t, 1H, -Ph), 6.93 (t, 1H, -Ph), 6.81(m, 2H, -Ph), 6.48 (d, 1H, -Ph), 6.04 (d, 1H, -Ph). ^{13}C NMR (400 MH$_Z$, $CDCl_3$): δ (ppm) 172.1, 169.0, 167.4, 148.8, 147.8, 146.7, 140.4, 137.1, 136.9, 136.7, 132.7, 132.4, 130.4, 129.2, 128.7, 127.4, 127.3, 127.2, 127.1, 126.9, 126.8, 126.3, 126.2, 125.8, 125.3,

125.1, 124.5, 123.0, 121.3, 121.0, 120.9, 120.8, 117.6, 117.3. ESI-MS (in CH_2Cl_2): *m/z*: 729.11 (100%; $[M-H]^+$).

For the third eluted **[Ir(ppy)$_2$(pic)]** (Yellow powders; R_f = 0.33): Yield: 66 mg (20%). Calcd for $C_{28}H_{20}IrN_3O_2$: C, 54.01; H, 3.24; N, 6.75%. Found: C, 54.06; H, 3.19; N, 6.77%. ^{1}H NMR (400 MHz, $CDCl_3$): δ (ppm) 8.81 (d, 1H, -Py), 8.30 (t, 1H, -Py), 7.80 (d, 2H, -Py), 7.72 (t, 1H, -Py), 7.44 (d, 2H ,-Py), 7.32 (t, 1H, -Py), 7.11 (t, 2H, -Ph), 6.82 (t, 2H, -Ph), 6.78 (t, 2H, -Py),6.71 (t, 2H, -Ph), 6.42 (d, 2H, -Py), 6.10 (d, 2H, -Ph). ESI-MS (in CH_2Cl_2) *m/z*: 623.12 (100%), $[M-H]^+$. This characterization result was identical to those in the literature.[32]

Synthesis and isolation of the [Ir(iqbt)(ppy)(Br-pic)] (2)

The synthesis and isolation of the [Ir(iqbt)(ppy)(Br-pic)] (**2**) followed in the same way as the [Ir(iqbt)(ppy)(pic)] (**1**) except that the **Br-Hpic**-ancillary ligand (170 mg, 1.10 mmol) was used in replacement with the **Hpic**-ancillary ligand (170 mg, 1.10 mmol).

For the first eluted **[Ir(iqbt)$_2$(Br-pic)]** (deep-red polycrystalline solid; R_f = 0.75): Yield: 70 mg (27%). Calcd for $C_{40}H_{23}BrN_3O_2S_2Ir$: C, 52.57; H, 2.54; N, 4.60%. Found: C, 52.58; H, 2.57; N, 4.58%. FT-IR (KBr cm-1): 3065 (w), 2887 (w), 2901 (w), 2359 (w), 2522 (w), 1734 (w), 1717 (w), 1684 (w), 1653 (s), 1616 (w), 1582 (m), 1558 (w), 1576 (m), 1541 (m), 1506 (m), 1474 (w), 1456 (w), 1437 (m), 1418 (vs), 1404 (m), 1364 (w), 1341 (m), 1307 (m), 1277 (w), 1233 (m), 1159 (w), 1128 (w), 1065 (w), 1045 (w), 1020 (w), 966 (w), 914 (m), 862(m), 841 (w), 812 (m), 770 (w), 756 (w), 735 (vs), 721 (m), 687 (vs), 661 (m), 637 (w), 567 (w), 529 (w), 501 (w).^{1}H NMR (400 MH_Z, $CDCl_3$): δ (ppm) 9.02 (d, 1H, -Py for iqbt), 8.94 (d, 1H, -Py for iqbt), 8.60 (d, 1H, -Py for Br-pic), 8.33 (s, 1H, -Py for Br-pic), 7.86 (d, 1H, -Pyfor iqbt), 7.81 (d, 1H, -Py for iqbt), 7.73 (m, 5H, -Ph), 7.64 (d, 1H, -Py for Br-pic), 7.38 (m, 2H, -Ph), 7.32 (d, 1H, -Ph), 7.26 (d, 1H, -Ph), 7.12 (d, 2H, -Ph), 7.00 (t, 1H, -Ph), 6.72 (t, 1H, -Ph), 6.56 (t, 1H, -Ph), 6.40 (d, 1H, -Ph), 6.00 (d, 1H, -Ph). ESI-MS (in CH_2Cl_2) *m/z*: 913.00 (100%), $[M-H]^+$.

For the second eluted [Ir(iqbt)(ppy)(Br-pic)] (**2**; reddish orange polycrystalline solid; R_f = 0.56): Yield: 44 mg (23%). Calcd for $C_{34}H_{21}N_3O_2BrSIr$: C, 50.56; H, 2.62; N, 5.20%. Found: C, 50.61; H, 2.59; N, 5.23%. FT-IR (KBr cm^{-1}): 3373 (b), 3064 (w), 2922 (w), 2848 (w), 1722 (w), 1645 (s), 1605 (w), 1582 (m), 1543 (w), 1502 (w), 1477 (w), 1454 (w), 1438 (m), 1418 (s), 1317 (m), 1261 (w), 1234 (w), 1161 (w), 1128 (w), 1097 (w), 1065 (w), 1031 (m), 1022 (m), 970 (w), 920 (w), 860 (m), 800 (m), 758 (s), 729 (vs), 688 (s), 663 (w), 631 (w), 565 (w), 519 (w), 430 (w). ^{1}H NMR (400 MH_Z, $CDCl_3$): δ 9.04 (d, 1H, -Py), 8.91 (d, 1H, -Py), 8.50 (d, 1H, -Py for Br-pic), 7.96 (d, 1H, -Py), 7.88 (d, 1H, -Py), 7.83 (t, 1H, -Py), 7.74 (m, 3H, -Py), 7.65 (d, 1H, -Ph), 7.52 (m, 2H, -Ph), 7.24 (t, 1H, -Ph), 7.15 (m, 3H, -Ph), 6.96 (t, 1H, -Ph), 6.80 (t, 2H, -Ph), 6.46 (d, 1H, -Ph), 6.00 (d, 1H, -Ph). ^{13}C NMR (400 MH_Z, $CDCl_3$): δ (ppm) 170.3, 168.8, 163.7, 153.5, 151.7, 149.1, 147.8, 145.2, 143.5, 143.2, 142.8, 140.3, 137.1, 136.0, 134.1, 132.7, 132.3, 130.8, 130.7, 130.5, 128.7, 126.9, 126.3, 125.8, 125.2, 125.1, 123.7, 123.1, 121.0, 121.3, 121.0, 120.9, 118.4, 117.5. ESI-MS (in CH_2Cl_2): *m/z*: 809.01 (100%; $[M+H]^+$).

For the third eluted **[Ir(ppy)$_2$(Br-pic)]** (yellow powder; R_f = 0.40): Yield: 62 mg (31%). Calcd for $C_{28}H_{19}BrIrN_3O_2$: C, 47.93; H, 2.73; N, 5.99%. Found: C, 48.00; H, 2.74; N, 6.02%.^{1}H NMR (400 MHz, CD_2Cl_2): δ (ppm) 8.69 (d, 1H, -Py), 8.44 (d, 1H, -Py), 7.96 (d, 1H, -Py), 7.90 (d, 1H, -Py), 7.81-7.75 (m, 2H, -Py), 7.67 (m, 2H, -Py), 7.59 (d, 1H, -Py), 7.56 (d, 1H, -Ph), 7.50 (m, 1H, -Ph), 7.18 (m, 1H, -Py), 7.03 (td, 1H, -Py), 6.96 (m, 2H, -Ph), 6.81 (m, 2H, -Ph), 6.20 (d, 1H, -Ph), 6.39 (d, 1H, -Ph). ESI-MS (in CH_2Cl_2): *m/z*: 702.59 (100%; $[M+H]^+$). This characterization result was identical to those in the literature.[33]

Theoretical calculation and experimental determination on the TDMs of NIR-emitters 1-2 and their EMLs

The calculations of the TDM vectors ($\vec{\mu}$-S_0, $\vec{\mu}$-T_1 and $\vec{\mu}$-($T_1 \rightarrow S_0$)) for the C_1-symmetric [Ir(C^N^1)(C^N^2)(N^O)-*tris*-heteroleptic Ir(III)-complexes [Ir(iqbt)(ppy)(pic)] (**1**) and [Ir(iqbt)(ppy)(Br-pic)] (**2**) were performed by DFT single point energy calculations using the hybrid functional B3LYP with the def2tzvp basis set based on their corresponding optimized T_1 and S_0 states. As to the experimental determination of molecular orientation of their doped EMLs, it was investigated by variable-angle spectroscopic ellipsometry (VASE) method. The DCM solution (10 mg/mL) of the mixture of PVK (poly-(*N*-vinylcarbazole), OXD7 (1,3-*bis*(5-(4-*tert*-butyl-phenyl)-1,3,4-oxadiazol-2-yl)benzene) and one of the C_1-symmetric [Ir(C^N^1)(C^N^2)(acac)]-*tris*-heteroleptic Ir(III)-complexes **1**-**2** with a stipulated wt% ratio of 65:30:5 as the EML was prepared under a N_2 atmosphere and spin-coated (at 2100 rpm) on the Si wafer substrate with a thickness of 50 nm. The EMLs also with the 50 nm thickness like their **NIR-PLEDs-1-2** were spin-coated onto a Si wafer substrate treated with a piranha solution for the VASE (EC-400 (M2000U), J. A. Woollam *Co*.) measurement.

Structural design of the NIR-PLEDs-1-2

Using a mixture PVK, OXD7 and one of the C_1-symmetric [Ir(C^N^1)(C^N^2)(N^O)]-*tris*-heteroleptic Ir(III)-complexes **1**-**2** with a stipulated wt% ratio of 65:30:5 as the EML, each of the **NIR-PLEDs-1-2** was fabricated with the same configuration of ITO/PEDOT:PSS (50 nm)/PVK:OXD7:Ir(III)-complex (50 nm)/TmPyPB (45 nm)/LiF (1nm)/Al (100 nm). In these materials, PEDOT:PSS (poly(ethylenedioxythiophene):poly(styrenesulfonate)) functioned as the hole-injecting material. TmPyPB (1,3,5-tri[(3-pyridyl)-phen-3-yl]benzene) was used to serve as the interface-modified function[34] of both electron-transport and hole-block. Details of the **NIR-PLEDs-1-2** fabrication and their testing are presented in the ESI.

3. Results and discussion

Synthesis and characterization of the C_1-symmetric [Ir(C^N^1)(C^N^2)(N^O)]-*tris*-heteroleptic Ir(III)-complexes 1-2

Also as shown in **Scheme 1**, the two-step procedure was adopted for the synthesis of each of the C_1-symmetric [Ir(C^N^1)(C^N^2)(N^O)]-*tris*-heteroleptic Ir(III)-complexes **1**-**2**. First, based on the straightforward metalation of the HC^N^1 ligand **Hiqbt** and the HC^N^2 ligand **Hppy** in an equimolar ratio with $IrCl_3{\cdot}3H_2O$, the μ-chloro-bridged dimer intermediates were obtained, where the **[Ir(iqbt)(ppy)(μ-Cl)]$_2$** intermediate was not isolated from the

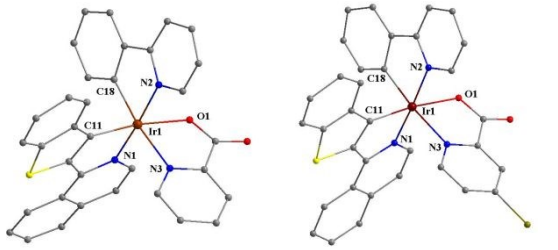

Figure 1 Perspective drawing of the [Ir(C^N^1)(C^N^2)(N^O)]-*tris*-heteroleptic mononuclear framework in **1** (left) and **2**·2$CHCl_3$ (right); H atoms, most labels and/or solvate were omitted for clarity.

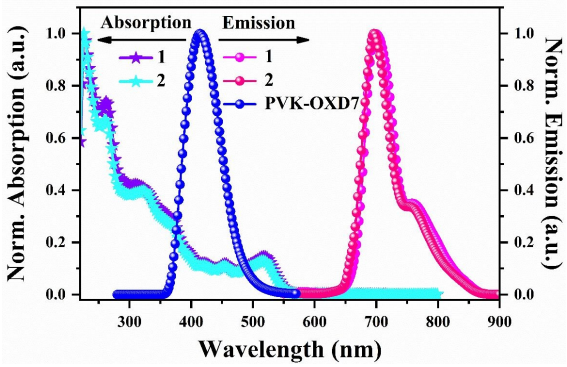

Figure 2 The normalized UV-visible-NIR absorption and photo-luminescence spectra of the Ir(III)-complexes **1**-**2** in solution (λ_{ex} = 375 nm) and the PVK-OXD-7 (65:30; weight ratio) in solid-state film (λ_{ex} = 273 nm) at room temperature.

inevitable interferents (**[Ir(iqbt)$_2$(μ-Cl)]$_2$** and **[Ir(ppy)$_2$(μ-Cl)]$_2$**). In the second step, treatment of the μ-chloro-bridged dimer intermediates with **Hpic** or **Br-Hpic** as the N^O ancillary ligand in the presence of *t*-BuOK, two [Ir(C^N^1)(C^N^2)(N^O)]-*tris*-heteroleptic Ir(III)-complexes [Ir(iqbt)(ppy)(pic)] (**1**) and [Ir(iqbt)(ppy)(Br-pic)] (**2**) as the targeted products were obtained, respectively. Worthy of noting, during the column chromatographic separation, two kinds of corresponding by-products (**[Ir(iqbt)$_2$(pic)]** and **[Ir(ppy)$_2$(pic)]**; **[Ir(iqbt)$_2$(Br-pic)]** and **[Ir(ppy)$_2$(Br-pic)]**) with different polarities were also isolated, respectively. Evidently, after the structural identification especially with the ^{1}H NMR result (**Figure S1**) on the typical [Ir(C^N)$_2$(N^O)]-*bis*-heteroleptic character, their formation is relied on the **[Ir(iqbt)$_2$(μ-Cl)]$_2$** and **[Ir(ppy)$_2$(μ-Cl)]$_2$** accompanied. However, probably due to the better solubility than all the [Ir(C^N)$_2$(N^O)]-*bis*-heteroleptic Ir(III)-complexes in common organic solvents, there has an acceptable yield for either [Ir(C^N^1)(C^N^2)(N^O)]-*tris*-heteroleptic **1** or **2** with the C_1-symmetry. The Ir(III)-complexes **1**-**2** were well-characterized by EA, FT-IR, ^{1}H/^{13}C NMR (**Figures S1-2**) and ESI-MS (**Figure S3**). In the ^{1}H NMR spectra, besides the combined proton resonances (δ = 9.05-6.04 ppm for **1** or 9.04-6.00 ppm for **2**) of the C^N^1 ligand (**iqbt**)$^-$, the C^N^2 ligand (**ppy**)$^-$ and the specific N^O ancillary ligand ((**pic**)$^-$ or (**Br-pic**)$^-$), their integration ratio is the stipulated 1:1:1 corresponding to their chemical formula. Meanwhile, in contrast to the resonance peak (δ = 8.65 ppm) of one proton on the C atom adjacent to the N atom in the free **Hiqbt**, the same characteristic protons peaking at *ca*. 9.05 ppm for the Ir(III)-complexes **1**-**2** give the signficant down-shifts, which should be attributed to the Ir(III)-induced coordination. Moreover, besides the characteristic chemial shift for the proton on the C atom adjacent to the N atom in the pyridyl ring of every (**ppy**)$^-$ located at *ca*. 7.96 ppm, the absence of the typical intra-molecular resonance-assisted hydrogen binding (RAHB, O-H$\cdots$N) signal to the free N^O ancillary ligand (**Hpic** or **Br-Hpic**), also verifies their multi-ligands' redistribution. The C_1-symmetric molecular structure of the two Ir(III)-complexes was further confirmed by the X-ray crystallography analyses (**Tables S1-2**) with **1** and **2**·2CHCl$_3$. As shown in **Figure 1**, one (**iqbt**)$^-$ ligand and one (**ppy**)$^-$ ligand with the similar C^N chelation (C11^N1 or C18^N2) mode, furnishing the *cis*-C,C and *trans*-N,N chelating disposition, while one (**pic**)$^-$ for **1** or one (**Br-pic**)$^-$ for **2**·2CHCl$_3$ with the N^O-chelate (N3^O1) mode coordinate to one Ir(III)-centre in a distorted octahedral geometry, leading to the [Ir(C^N^1)(C^N^2)(N^O)-*tris*-heteroleptic mononuclear framework. In comparison, the (**Br-pic**)$^-$-incorporation in the Ir(III)-complex **2** has the minor influence on the Ir-C, Ir-N and Ir-O bond lengths, and does not change the *co*-planar character of each of the three different ligands compared to the (**pic**)$^-$-involved Ir(III)-complex **1**. However, the Br-electron-drawing effect induces the distinctively different dihedral angles of 38.1(2)°, 83.9(3)° and 86.6(3)° for the Ir(III)-complex **2** while 88.4(3)°, 85.4(3)° and 75.1(3)° for the Ir(III)-complex **1** among every two ligand-based planes, correspondingly, indicative of the differential multi-ligands' alignment regulated by the specific N^O-chelate ancillary ligand. Thermogravimetric analysis (TGA; **Figure S4**) of the Ir(III)-complexes **1**-**2** shows that a relatively higher 5% weight-reduction temperature of 339 °C for **1** than that (315 °C) for **2**, while their thermal stability is sufficient enough to the following device fabrication.

Theoretical calculation and experimental photo-physical property determination of the C_1-symmetric [Ir(C^N^1)(C^N^2)(N^O)]-*tris*-heteroleptic Ir(III)-complexes 1-2

The absorption and photo-luminescence spectra of the Ir(III)-complexes **1**-**2** were determined in solution, and the result was summarized in **Table S3** and **Figure 2**. As shown in **Figure 2**, evidently different from the limited absorptions (**Figure S5**) of λ_{ab} < 400 nm of the ligands, the Ir(III)-complexes **1**-**2** and the four by-products (**Figure S6**) show the significantly broadened UV-visible-NIR absorptions. The strong high-energy absorption bands (λ_{ab} = 200-430 nm) should be arisen from the intraligand spin-allowed $^1\pi$-π^* transitions, the moderate absorptions within the lower-energy region (λ_{ab} = 430-600 nm; 518 nm for **1** or 516 nm for **2**) attributed to the mixed ^{1,3}LLCT/^{1,3}MLCT (LLCT = ligand-to-ligand charge transfer) transitions, and the relatively weak bands extending over 600 nm probably assigned to the ground-state excitation into the lowest triplet state ($S_0 \rightarrow T_1$) are observed, respectively. Noticeably, besides the comparable absorptions of the Ir(III)-complexes **1**-**2**, the introduction of **Hpic**/**Br-Hpic** ancillary also gives rise to the minor effect on their photo-luminescent spectra, in which, upon photo-excitation (λ_{ex} = 375 nm), the almost similar strong NIR-emissions (also **Figure 2**) peaking at 699 nm and a shoulder at 760 nm for **1** *versus* peaking at 697 nm and a differentiable shoulder around 754 nm for **2** are observed, respectively. In sharp contrast to the rigidochromic fluorescence (**Figure S7**) of the ligands or the visible-light (**Figure S8**) of **[Ir(ppy)$_2$(pic)]** (λ_{em} = 507 nm) or **[Ir(ppy)$_2$(Br-pic)]** (λ_{em} = 587 nm), the exclusively strong NIR-emissions characteristic of the typically phosphorescent nature (τ = 0.34 μs at λ_{em} = 699 nm (**1**) or 0.35 μs at λ_{em} = 697 nm (**2**)), should result from the effective Dexter[35] energy transfer for the Ir(III)-complexes **1**-**2**. Interestingly, the NIR-phosphorescent lifetimes are significantly shorter than those (τ ~ 1.0 μs) of the C_3-*fac*-[Ir(iqbt)$_3$]-homoleptic[23c] and [Ir(iqbt)$_2$(L^X)]-*bis*-heteroleptic[24f-24g] counterparts (included **[Ir(iqbt)$_2$(pic)]**/**[Ir(iqbt)$_2$(Br-pic)]**); also **Figure S8**), which should be due to a restrictive vibronic motion to the NIR-emissive excited state of the C_1-symmetric [Ir(C^N^1)(C^N^2)(N^O)]-*tris*-heteroleptic Ir(III)-complexes **1**-**2**. Accordingly, this situation can be reflected from their vibronically structural while almost identical NIR-emissions with the small S_M (Huang-Rhys factor; 0.31) at room temperature or 77 K (0.28 for **1** (698 and 764 (sh) nm); 0.30 for **2** (696 and 760 (sh) nm). However, the slightly higher Φ_{PL} of 0.27 for **1** than that (0.21) of **2** is checked, which can be confirmed from its relatively larger k_r (7.9×10^5 s^{-1}) value and the almost equivalent k_{nr} one (2.1×10^6 s^{-1}) compared to the Ir(III)-complex **2** ($k_r = 2.3\times10^5$ s^{-1}).

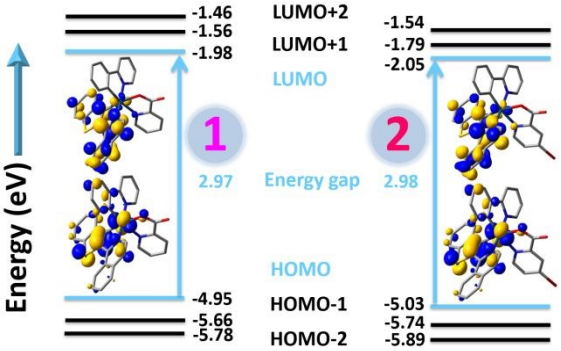

Figure 3 The HOMO and LUMO patterns for the Ir(III)-complexes **1**-**2** based on their optimized S_0 geometries.

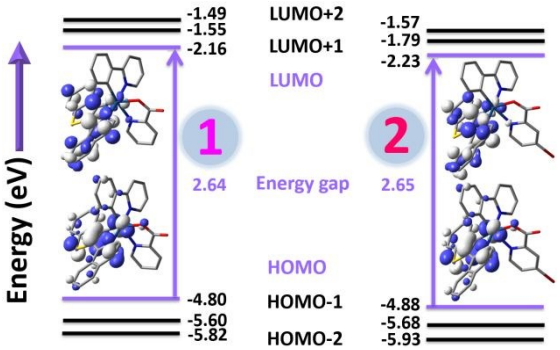

Figure 4 The HOMO and LUMO patterns for the Ir(III)-complexes **1**-**2** based on their optimized T_1 geometries.

To understand the **Br-Hpic**/**Hpic**-incorporated electronic effect on the differential photophysical property of their Ir(III)-complexes **1**-**2**, DFT/TD-DFT calculations based on their optimized S_0 and T_1 geometries were explored, respectively. As shown in T**able S4** and **Figure 3** for the S_0-optimized DFT result, the Ir(III)-complexes **1**-**2** have the similar distribution patterns to all the HOMOs and the LUMOs. Especially besides the most contribution (ca. 92%) from the C^N^1 ligand ((**iqbt**)$^-$) to the LUMO, the HOMO is mainly located at the C^N^1 ligand ((**iqbt**)$^-$) and the Ir(III) centre (53.24% and 28.62% for **1**; 54.18% and 28.05% for **2**), accompanied by some contribution (15.04% for **1**; 14.84% for **2**) from the C^N^2 ligand ((**ppy**)$^-$). Accordingly, despite the minor portion (3.11%/1.78% for **1**; 2.94%/2.92% for **2**) to the HOMO/LUMO while the pronounced one (89.39% for **1**; 94.49% for **2**) to the LUMO+1 from the N^O-ancillary ((**pic**)$^-$ or (**Br-pic**)$^-$), the (**Br-pic**)$^-$-incorporation in Ir(III)-complex **2**, due to the Br-electron-withdrawing effect, induces the slightly larger contributions to the LUMO/LUMO+1 while the slightly reduced contributions to the HOMO compared to the ((**pic**)$^-$)-involved Ir(III)-complex **1**. Therefore, considering the dominated HOMO $\rightarrow$ LUMO transition for the $S_0 \rightarrow S_1$ (ca. 95%) or the $S_0 \rightarrow T_1$ (ca. 86%) excitation, for the Ir(III)-complexes **1**-**2**, the visible absorption (λ_{ab} = 430-600 nm; 518 nm for **1** or 516 nm for **2**) is mainly caused by the ^{1}LC/^{1}MLCT-admixed transitions (^{1}ILCT (34.99%), ^{1}LLCT (22.51%) and ^{1}MLCT (36.60%) for **1**; ^{1}ILCT (35.47%), ^{1}LLCT (22.53%) and ^{1}MLCT (36.20%) for **2**), and the $S_0 \rightarrow T_1$ transited lowest-energy absorption is mostly attributed to the ^{3}ILCT transition (70.73% for **1**; 71.47% for **2**) mixed with the less ^{3}MLCT one (17.11% for **1**; 16.62% for **2**). On the other hand, based on the T_1-optimized TD-DFT calculation result (**Tables S5-S6** and **Figure 4**) for the two Ir(III)-complexes **1**-**2**, besides the consistent HOMOs/LUMOs distribution pattern, the domination (95.3% for **1**; 93.4% for **2**) of the HOMO $\rightarrow$ LUMO transition shows that their NIR-phosphorescence is characteristic of the ^{3}LC/^{3}MLCT-admixed nature with the ^{3}LC-dominant. However, the electron-withdrawing (**Br-pic**)$^-$-incorporation stabilizes both the HOMO (-4.88 eV) and the LUMO (-2.23 eV) of its Ir(III)-complex **2** in comparison to those (-4.80 and -2.16 eV) of the Ir(III)-complex **1**, resulting in their comparable HOMO-LUMO bandgap (2.65/2.64 eV). Nonetheless, the augmented (20.24%) ^{3}MLCT character in the Ir(III)-complex **1** compared to that (19.93%) in the Ir(III)-complex **2** should be one of the reasons to the slightly higher Φ_{PL} of **1** than that of **2**.

To further explore the k_r-relative TDM effect on the Φ_{PL}, both the $\vec{\mu}$-S_0 and the $\vec{\mu}$-T_1 dipole moment vectors of the Ir(III)-complexes **1**-**2** were investigated (**Table S7** and **Figure 5**) upon DFT calculations based on their corresponding S_0/T_1-optimized states, respectively. Contributing from the C_1-symmetry of the Ir(III)-complexes **1**-**2**, the directions of the $\vec{\mu}$-S_0 (5.77 Debye for **1**; 5.35 Debye for **2**) and the $\vec{\mu}$-T_1 (5.80 Debye for **1** and 5.54 Debye for **2**) dipole moment vectors are differential, from which significantly different from the identical C_2-axis located for typical C_2-[Ir(C^N)$_2$(L^X)-bis-heteroleptic Ir(III)-complexes, the equivalent θ angle of 22° between every two corresponding vectors gives rise to the slightly larger $\vec{\mu}$-($T_1 \rightarrow S_0$) size (2.24 Debye) of **1** than that (2.12 Debye) of **2**. Accordingly, returning to $k_r \in$ TDM^2 ruled by the electronic transition theory,[30] the well-verified larger k_r forward a desirably higher Φ_{PL} for the Ir(III)-complex **1** is understandable. Undoubtedly, the specific TDM orientation motivated from the C_1-symmetric Ir(III)-complexes **1**-**2** is available for the promoted photo-luminescence, while its extension beneficial to the electroluminescence or not, needs to be further confirmed (*vide infra*).

Structure design and performance of NIR-PLEDs based on the C_1-symmetric Ir(III)-complexes 1-2

In consideration of the efficient NIR-phosphorescence of the C_1-symmetric Ir(III)-complexes **1**-**2**, it is of interest on low-cost and scalable NIR-PLEDs applications. In the beginning, their experimental HOMO/LUMO levels were checked from the electrochemical behaviours. As shown in the **Figure S9**, each of the C_1-symmetric Ir(III)-complexes **1**-**2** exhibits the reversible oxidation and reduction waves. In the oxidation process (HOMO-level stabilization), the anodic shift with +0.51 V (**1**) or +0.53 V (**2**) versus Fc^+/Fc is observed, which should be attributed to the oxidation of

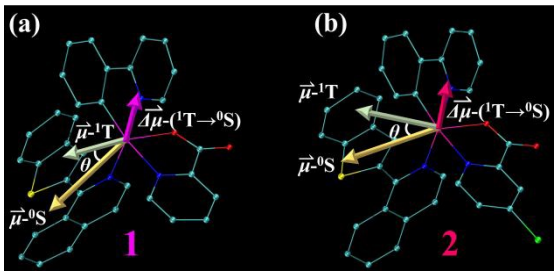

Figure 5 The TDM (transition dipole moment) vectors of the Ir(III)-complexes **1**-**2** based on their optimized and S_0 and T_1 geometries.

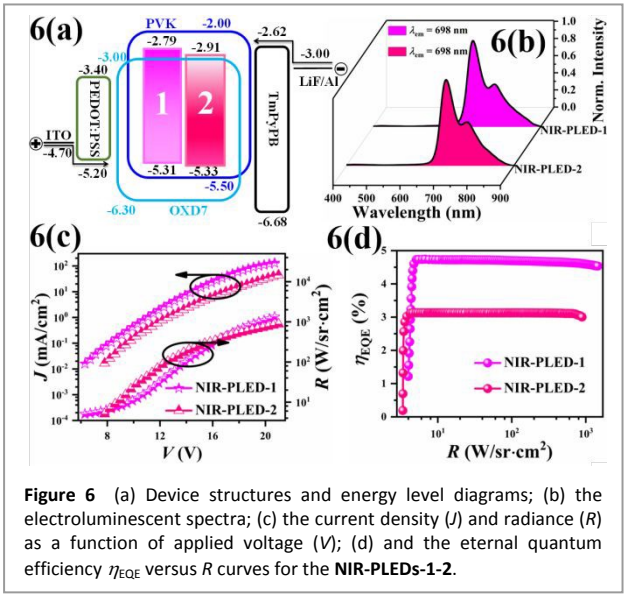

Figure 6 (a) Device structures and energy level diagrams; (b) the electroluminescent spectra; (c) the current density (*J*) and radiance (*R*) as a function of applied voltage (*V*); (d) and the eternal quantum efficiency η_{EQE} versus *R* curves for the **NIR-PLEDs-1-2**.

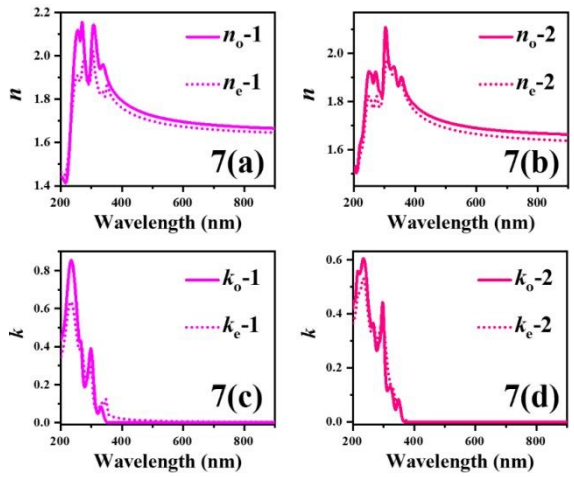

Figure 7 Wavelength-relative refractive indices (*n*; a-b) and coefficients (*k*; c-d) in ordinary (n_o/k_o) and extraordinary (n_e/k_e) modes of the EML-**1** and EML-**2** doped with the corresponding Ir(III)-complexes **1**-**2**.

the predominant (**iqbt**)$^-$ moiety together with the Ir(III)-centre involved. During the reduction (LUMO-level stabilization), the first one-electron reduction process localizes on the (**iqbt**)$^-$ portion at -2.01 V for **1**, which is anodically shifted by 0.12 V compared to -1.89 V for **2**. Accordingly, both the HOMO and the LUMO of the Ir(III)-complex **2** (-5.33/-2.91 eV) are stabilized in comparison with those of (-5.31/-2.79 eV) the Ir(III)-complex **1**, in good agreement with the result by DT-DFT calculations. Thanks to PVK-OXD7 with the good hole/electron transport,[24] the practical LUMO/HOMO levels of the C_1-symmetric Ir(III)-complexes **1**-**2** perfectly within those of PVK-OXD7, also suggests their suitability to desirable solution-processed NIR-PLEDs.

As shown in **Figure 6**, using the C_1-symmetric Ir(III)-complexes **1**-**2** as the dopants at a 5% wt% level in PVK-OXD7 (65:30, wt%), **NIR-PLEDs-1-2** with the same configuration (**Figure 6(a)**) were fabricated, respectively. Just as expected, up illumination shown in **Figure 6(b)**, the **NIR-PLEDs-1-2** exhibit the Ir(III)-complex-related NIR-emissions well resembled those (also **Figure 2**) for the C_1-symmetric Ir(III)-complexes **1**-**2** in solution. Meanwhile, under a proper forward bias, their almost consistent (λ_{em} = 698 nm) electroluminescent spectra are independent on the applied voltage. The absence of either the ligands or PVK-OXD7 fluorescence indicates that apart from Dexter energy transfer,[35] effective Förster[36] energy transfer (deduced from the significant spectral overlap between the emission of PVK-OXD7 with the MLCT-transited absorption of **1**-**2** also shown in Figure **2**) from PVK-OXD7 to the dopant occurs during the carrier-trapping process. Moreover, by checking the *J*-*V*, *R*-*V* and η_{EQE}-*R* curves shown in **Figures 6(c)/6(d)**, in accordance with an increase of the *V*, both the *J* and *R* monotonously increase, while the η_{EQE} increase instantly and then decreases steadily during the following operation, giving the J^{Max} of 138.9 mA/cm^2 or 44.2 mA/cm^2, the R^{Max} of 1433.6 W/sr·cm^2 or 877.0 W/sr·cm^2 to the **NIR-PLEDs-1-2**, respectively. For comparison, besides the 1.6-fold time irradiance of **NIR-PLED-1** in relative to **NIR-PLED-2**, the superior performance of the **NIR-PLED-1** is reflected from the lower V_{on} (the voltage of *R* = 5 W/sr·cm^2) of 6.3 V and the larger η_{EQE}^{Max} of 4.7% than those (7.8 V of V_{on} and η_{EQE}^{Max} of 3.1% of the **NIR-PLED-2** apart from the similarly negligible (< 5%) efficiency roll-off. The slightly lower V_{on} in accompany with the larger *R* for the **NIR-PLED-1** can be assigned to the relatively smaller LUMO energy barrier between the NIR-emitter **1** and TmPyPB towards a promoted electron-transport. As to the reason to its 1.5-fold increasing of η_{EQE}^{Max} for the **NIR-PLED-1** compared to the **NIR-PLED-2**, it seems incomprehensible just from the Φ_{PL}-mirrored (Φ_{PL} of 0.27 for **1** versus 0.21 for **2**) trend.

After following the TmPyPB-assisted electron/hole mobility compatible with our device configuration as the literature,[24f] the effect of the comparable η_{eh} on the differential η_{EQE} for the **NIR-OLED-1/2** could be temporarily ignored. According, as a key point to η_{out}, the NIR-light extraction arisen from molecular orientation should be concentrated. Towards its resolution, the orientation distribution the EMLs' films (EML-**1** and EML-**2**) used for the **NIR-PLED-1/2** was quantitatively studied by the VASE method, and the resultant ordinary/extraordinary refractive index (n_o/n_e) and coefficient (k_o/k_e) results were summarized in **Table S8** and **Figure 7**. Along with the θ' (angle between the TDM vector and the direction vertical to the substrate) waving of 58.61° for the EML-**1** or 55.51° for the EML-**2**, the corresponding order parameter *S* of -0.093 for the EML-**1** or -0.043 for the EML-**2** is founded, and thus, the horizontal dipole ratio (h/(h+v); 73.0% (EML-**1**) versus 69.5% (EML-**2**)) exceeding 69% is approached. Therefore, in contrast to the isotropic mode of *S* = 0, effective NIR-light out-coupling should occur. Despite the anisotropic orientation mechanism difficult to be revealed with the complicated binding between PVK-OXD7 and the dopant, the more preferentially horizontal orientation parallel to the substrate of the EML-**1** than that of the EML-**2**, should be substantially beneficial for the higher efficiency of the **NIR-PLED-1** compared to the **NIR-PLED-2**. Encouragingly, in consideration of the record η_{EQE}^{Max} of 3.1-4.7% for the **NIR-PLEDs-1-2** among previously solution-processed NIR-OLEDs/PLEDs and even the top-level within vacuum-deposited NIR-OLEDs based on reported Ir(III)-complexes,[23-24] this work paves an available avenue to develop [Ir(C^N^1)(C^N^2)(N^O)]-*tris*-heteroleptic Ir(III)-complexes suitable for low-cost scalable NIR-PLEDs.

4. Conclusions

In summary, through the molecular design of the C_1-symmetric [Ir(C^N^1)(C^N^2)(N^O)]-*tris*-heteroleptic Ir(III)-complexes **1**-**2**, their good NIR-phosphorescence is confirmed from the strengthened ^{3}MLCT effect and the large TDM. Moreover, as a result of their

doped EMLs with the preferentially horizontal orientation towards reliable NIR-PLEDs, the superior device performance (η_{EQE}^{max} of 3.1-4.7% and negligible (< 5%) efficiency roll-off), renders C_1-symmetric [Ir(C^N^1)(C^N^2)(N^O)]-*tris*-heteroleptic Ir(III)-complexes a new platform for cost-effective and large-area flexible NIR-PLEDs.

Conflicts of interest

There are no conflicts to declare.

Acknowledgements

This work was funded by the National Natural Science Foundation (21373160, 21173165, 22001212), the State Key Laboratory of Structure Chemistry (20190026), the Guangdong Basic and Applied Basic Research Foundation (2019A1515110527), the Hong Kong Research Grants Council (PolyU153058/19P), the Hong Kong Polytechnic University (1-ZE1C and YW4T) and the Endowed Professorship in Energy from Ms. Clarea Au (847S) in China.

Notes and references

1 C. Ulbricht, B. Beyer, C. Friebe, A. Winter and U. S. Schubert, *Adv. Mater.*, 2009, **21**, 4418-4441.
2 T. Y. Li, J. Wu, Z. G. Wu, Y. X. Zheng, J. L. Zuo and Y. Pan, *Coord. Chem. Rev.*, 2018, **374**, 55-92.
3 (a) A. F. Henwood and E. Zysman-Colman, *Chem. Commun.*, 2017, 53, 807-826; (b) F. Xu, H. U. Kim, J.-H. Kim, B. J. Jung, A. C. Grimsdale and D.-H. Hwang, *Prog. Polym. Sci.*, 2015, **47**, 92-121.
4 S. Lee and W.-S. Han, *Inorg. Chem. Front.*, 2020, **7**, 2396-2422.
5 G. Z. Lu, L. Liu, Z. L. Tu, Y. H. Zhou and Y. X. Zheng, *J. Mater. Chem. C*, 2019, **7**, 2022-2028.
6 C.-L. Ho, H. Li and W.-Y. Wong, *J. Organomet. Chem.*, 2014, **751**, 261-285.
7 (a) A. Zampetti, A. Minotto and F. Cacialli, *Adv. Funct. Mater.*, 2019, **29**, 1807623; (b) M. Ibahim-Ouali and F. Dumur, *Molecules*, 2019, **24**, 1412.
8 H. F. Xiang, J. H. Cheng, X. F. Ma, X. G. Zhou and J. J. Chruma, *Chem. Soc. Rev.*, 2013, **42**, 6128-6185.
9 A. Barbieri, E. Bandini, F. Monti, V. K. Praveen and N. Armaroli, *Top. Curr. Chem.*, 2016, **374**, 1-39.
10 Y. Q. Zheng and X. Z. Zhu, *Org. Mater.*, 2020, **2**, 253-281.
11 K. Y. Zhang, S. J. Liu, Q. Zhao, F. Y. Li and W. Huang, *Struct. Bond.*, 2015, **165**, 131-180.
12 S.-Y. Kim, W.-I. Jeong, C. Mayr, Y.-S. Park, K.-H. Kim, J.-H. Lee, C.-K. Moon, W. Brütting and J.-J. Kim, *Adv. Funct. Mater.*, 2013, **23**, 3896-3900.
13 J. V. Caspar and T. J. Meyer, *J. Phys. Chem.*, 1983, **87**, 952-957.
14 K. Saxena, V. K. Jain and D. S. Mehta, *Opt. Mater.*, 2009, **32**, 221-233.
15 K. B. Choi, S. J. Shin, T. H. Park, H. J. Lee, J. H. Hwang, J. H. Park, B. Y. Hwang, Y. W. Park and B.-B. Ju, *Org. Electron.*, 2014, **15**, 111-117.
16 C. Y. Huang, Y. W. Zhang and X. P. Zhang, *Nanophoton.*, 2020, **9**, 2905-2913.
17 L. X. Xiao, Z. J. Chen, B. Wu, J. X. Luo, S. Kong, Q. H. Gong and J. Kido, *Adv. Mater.*, 2011, **23**, 926-952.
18 J. Song, H. Lee, E. G. Jeong, K. C. Choi and S. Yoo, *Adv. Mater.*, 2020, **32**, 1907539.
19 M. Flämmich, J. Frischeisen, D. S. Setz, D. Michaelis, B. C. Krummacher, T. D. Schmidt, W. Bruetting and N. Danz, *Org. Electron.*, 2011, **12**, 1663-1668.
20 C.-K. Moon, K.-H. Kim and J.-J. Kim, *Nat. Commun.*, 2017, **8**, 1-10.
21 M. J. Jurow, C. Mayr, T. D. Schmidt, T. Lampe, P. I. Djurovich, W. ing and M. E. Thompson, *Nat. Mater.*, 2016, **15**, 85-91.
22 K.-H. Kim and J.-J. Kim, *Adv. Mater.*, 2018, **30**, 1705600.
23 (a) Y. X. Zhang, Q. Li,M.H. Cai, J. Xue and J. Qiao, *J. Mater. Chem. C*, 2020, **8**, 8484-8492; (b) J. Xue, L. J. Xin, J. Y. Hou, L. Duan, R. J. Wang, Y. Wei and J. Qiao, *Chem. Mater.*, 2017, **29**, 4775-4782; (c) I. Shigeru, Y. Shigeyuki, M. Takeshi, N. Hiroyuki, F. Hideki, K. Shiro and S. Yoshiaki, *Inorg. Chem. Commun.*, 2013, **38**, 14-19.
24 (a) Z. Chen, H. Y. Zhang, D. W. Wen, W. H. Wu, Q. G. Zeng, S. M. Chen and W.-Y. Wong, *Chem. Sci.*, 2020, **11**, 2342-2349; (b) C. F. You, D. H. Liu, J. T. Yu, H. Tian, M. B. Zhu, B. Zhang, Y. Liu, Y. F. Wang and W. G. Zhu, *Adv. Opt. Mater.*, 2020, **8**, 2000154; (c) C. F. You, D. H. Liu, M. B. Zhu, J. T. Yu, B. Zhang, Y. Liu, Y. F. Wang and W. G. Zhu, *J. Mater. Chem. C.*, 2020, **8**, 7079-7088; (d) C. F. You, D. H. Liu, F. Y. Meng, Y. F. Wang, J. T. Yu, S. Wang, S. J. Su and W. G. Zhu, *J. Mater. Chem. C.*, 2019, **7**, 10961–10971; (e) H. U.Kim, S. Sohn, W. Choi, M. Kim, S. U. Ryu, T. Park, S. Jung and K. S. Bejoymohandas, *J. Mater. Chem. C.,* 2018, **6**, 10640-10658; (f) G. R. Fu, H. Zheng, Y. N. He, W. T. Li, X. Q. Lü and H. S. He, *J. Mater. Chem. C*, 2018, **6**, 10589-10596; (g) S. Kesarkar, W. Mróz, M. Penconi, M. Pasini, S. Destri, M. Cazzaniga, D. Ceresoli, P. R. Mussini, C. Baldoli, U. Giovanella and A. Bossi, *Angew. Chem. Int. Ed.*, 2016, **55**, 2714-2718; (h) X. S. Cao, J. S. Miao, M. R. Zhu, C. Zhong, C. L. Yang, H. B. Wu, J. G. Qin and Y. Cao, *Chem. Mater.*, 2015, **27**, 96-104.
25 C. Shi, H. Huang, Q. X. Li, J. W. Yao, C. C. Wu, Y. B. Cao, F. X. Sun, D. G. Ma, H. Yan, C. L. Yang and A. H. Yuan, *Adv. Opt. Mater.*, 2021, **9**, 2002060.
26 Y. H. Sun, X. L. Yang, Z. Feng, B. O. Liu, D. K. Zhong, J. J. Zhang, G. J. Zhou and Z. X. Wu, *ACS Appl. Mater. Interfaces*, 2019, **11**, 26152-26164.
27 J.-L. Liao, Y. Chi, Z.-T. Sie, C.-H. Ku, C.-H. Chang, M. A. Fox, P. J. Low, M.-R. Tseng and G.-H. Lee, *Inorg. Chem.*, 2015, **54**, 10811-10821.
28 W. P. Dang, X. L. Yang, Z. Feng, Y. H. Sun, D. K. Zhong, G. J. Zhou, Z. X. Wu and W.-Y. Wong, *J. Mater. Chem. C*, 2018, **6**, 9453-9464.
29 V. Adamovich, S. Bajo, P.-L. T. Boudreault, M. A. Esteruelas, A. M. López, J. Martín, M. Oliván, E. Oňate, A. U. Palacios, A. San-Torcuato, J.-Y. Tsai and C. Xia, *Inorg. Chem.*, 2018, **57**, 10744-10760.
30 L.-S. Cui, Y. Liu, X.-Y. Liu, Z.-Q. Jiang and L.-S. Liao, *ACS Appl. Mater. Interfaces*, 2015, **7**, 11007-11014.
31 G. N. Li, Y. Zou, Y. D. Yang, J. Liang, F. Cui, T. Zheng, H. Xie and Z. G. Niu, *J. Fluoresc.*, 2014, **24**, 1545-1552.
32 D. Gupta, M. Katiyar, T. Hazra, A. Verma, S. S. Manharan and A. Biswas, *Opt. Mater.*, 2006, **28**, 1356-1361.
33 R. Davidson, Y.-T. Hsu, C. Bhagani, D. Yufit and A. Beeby, *Organometallics*, 2017, **36**, 2727-2735.
34 X. L. Yang, G. J. Zhou and W.-Y Wong, *Chem. Soc. Rev.*, 2015, **44**, 8484-8575.
35 D. Wasserberg, S. C. J. Meskers and R. A, J. Janssen, *J. Phys. Chem. A*, 2007, **111**, 1381-1388.
36 D. R. Martir and E. Zysman-Colman, *Coord. Chem. Rev.*, 2018, **364**, 86-117.